The Blume-Emery-Griffiths Spin Glass Model

Mauro Sellitto ([1,*]), Mario Nicodemi ([1]) and Jeferson J. Arenzon ([2])

([1]) Dipartimento di Scienze Fisiche, Unità INFM, Università "Federico II", Mostra d'Oltremare, Pad. 19, 80125 Napoli, Italy
([2]) Instituto de Física, UFRGS, CP 15051, 91501-970, Porto Alegre, RS, Brazil

(Received 24 January 1997, revised 8 April 1997, accepted 28 April 1997)

PACS.75.10.Nr – Spin-glass and other random models
PACS.05.50.+q – Lattice theory and statistics; Ising problems
PACS.64.70.Pf – Glass transitions

Abstract. — The equilibrium properties of the Blume-Emery-Griffiths model with bilinear quenched disorder are studied for the case of attractive as well as repulsive biquadratic interactions. The global phase diagram of the system is calculated in the context of the replica symmetric mean field approximation.

1. Introduction

The Blume-Emery-Griffiths (BEG) [1] model has been successfully applied to explain the behavior of different physical systems such as He^3-He^4 mixtures, microemulsions, semiconductor alloys, to quote only a few. In this paper we investigate the effect of quenched disorder on the mean field phase diagram of a version of the BEG model in which orientational and particle degrees of freedom are explicitly introduced. We consider the Hamiltonian:

$$\mathcal{H} = -\sum_{i<j} J_{ij} S_i S_j n_i n_j - \frac{K}{N} \sum_{i<j} n_i n_j - \mu \sum_i n_i, \tag{1}$$

where $S_i = \pm 1$, $n_i = 0, 1$; the bilinear couplings J_{ij} are quenched Gaussian random variables with average J_0/N and variance J^2/N, and the sign of biquadratic interaction may be negative. This Hamiltonian represents a general framework to study the complex behavior of many physical systems. In the simple case of pure systems it describes, for example, a fluid model with magnetic properties like those of polar liquids, which exhibits multiple exotic phase diagrams [2–6]. In presence of quenched disorder the Hamiltonian (1) implements different models whose rich phase diagrams are not yet fully explored. Some limiting cases include the standard Ising spin glass [7] ($\mu \to \infty$; $n_i = 1\ \forall i$) and the Ghatak-Sherrington model [8–13] ($K = 0$). In the particular case of $K = -1$ we recover the Frustrated Ising Lattice Gas [14, 15] that is a version of the *Frustrated Percolation* model [16], whose properties suggest a possible close connection with the theories of *structural glasses* [17]. Essentially, the model considers a lattice gas in a frustrated medium where the particles have an internal degree of freedom (given by its spin)

(*) Author for correspondence (e-mail: sellitto@na.infn.it)

that accounts, for example, for possible orientations of complex molecules in glass forming liquids. These steric effects are greatly responsible for the geometric frustration appearing in glass forming systems at low temperatures or high densities. Besides that, the particles interact through a potential that may be attractive or repulsive depending on the value of K.

Here we try to further elucidate the phase diagram properties of Hamiltonian (1) within a replica mean field theory approach. Specifically, the presence of disorder in the bilinear term leads to the appearance of a transition from a paramagnetic to a spin glass phase at low temperature or high density. When the biquadratic interaction is attractive or weakly repulsive we found, accordingly with the value of density, two spin glass transitions of different nature separated by a tricritical line: at high density the transition is continuous while at sufficiently low density the transition becomes discontinuous. When the particle repulsion is rather strong two new phases with a sub-lattice structure may appear: an antiquadrupolar phase and at lower temperatures, an antiquadrupolar spin glass phase. The antiquadrupolar spin glass transition line is always continuous whatever is the value of the chemical potential. When the bond weights are not symmetrically distributed, a ferromagnetic phase (as well as a ferrimagnetic one, depending on the value of J_0) may appear in the phase diagram. One can also identify a line where a dynamical instability appears, as in spin glass models with discontinuous transition like the Potts glass [18, 19] and the p-spin model [17, 20]. Moreover, preliminary results on the stability analysis indicates the presence of a transition line from a 'phase' with one to a 'phase' with infinity replica symmetry breaking. This rich scenario and the unification picture provided by the model are the main motivations of this paper.

2. The Phase Diagram

Many general properties of the phase diagram of Hamiltonian (1) may be observed by simply studying the replica symmetric solutions of the mean-field equations. In the following paragraphs we discuss how the many thermodynamic phases appear when the parameters of Hamiltonian (1) are changed.

For the sake of clarity we work out separately the cases of attractive, $K > 0$, and repulsive, $K < 0$, biquadratic interaction.

2.1. Attractive Biquadratic Interaction. — Using the replica method the free energy can be computed as:

$$\beta f = -\lim_{n\to 0} \frac{1}{n} \ln[Z^n]_{\rm av}, \tag{2}$$

where n is the numbers of replicas and $[\cdots]_{\rm av}$ denotes the average over the disorder. We obtain:

$$\beta f = \lim_{n\to 0} \frac{1}{n} \left[\frac{1}{2}\beta^2 J^2 \sum_{a<b} q_{ab}^2 + \frac{1}{2}\beta J_0 \sum_a m_a^2 + \frac{1}{4}(\beta^2 J^2 + 2\beta K) \sum_a d_a^2 - \ln Z' \right], \tag{3}$$

where Z' is the single site partition function:

$$\begin{aligned} Z' = \operatorname*{Tr}_{S,n} \exp \Bigg\{ & \beta^2 J^2 \sum_{a<b} q_{ab} S^a n^a S^b n^b + \beta \sum_a J_0 m_a S^a n^a \\ & + \sum_a \left[\left(\frac{\beta^2 J^2}{2} + \beta K \right) d_a + \beta\mu \right] n^a \Bigg\}, \end{aligned} \tag{4}$$

and the order parameters: density (d_a), magnetization (m_a), and Parisi overlap (q_{ab}), are defined as

$$\begin{aligned} d_a &= \langle n^a \rangle , \quad (5) \\ m_a &= \langle S^a n^a \rangle , \quad (6) \\ q_{ab} &= \left\langle S^a n^a S^b n^b \right\rangle . \quad (7) \end{aligned}$$

In the replica symmetric approximation, $m_a = m$, $d_a = d$ and $q_{ab} = q(1 - \delta_{ab})$, one finds:

$$\begin{aligned} \beta f &= \frac{1}{2}\beta J_0 m^2 - \frac{1}{4}\beta^2 J^2 q^2 + \frac{1}{4}(\beta^2 J^2 + 2\beta K)d^2 \\ &\quad - \int \mathcal{D}z \, \ln 2 \left[1 + \mathrm{e}^{\Xi} \cosh(\beta J z \sqrt{q} + \beta J_0 m)\right] , \end{aligned} \quad (8)$$

where $\mathcal{D}z = \mathrm{d}z \mathrm{e}^{-z^2/2}$ is the standard Gaussian measure and we define:

$$\Xi \equiv \frac{\beta^2 J^2}{2}(d - q) + \beta K d + \beta \mu. \quad (9)$$

The order parameters satisfy the saddle point equations:

$$d = \int \mathcal{D}z \, \frac{\cosh(\beta J z \sqrt{q} + \beta J_0 m)}{\mathrm{e}^{-\Xi} + \cosh(\beta J z \sqrt{q} + \beta J_0 m)}, \quad (10)$$

$$q = \int \mathcal{D}z \, \frac{\sinh^2(\beta J z \sqrt{q} + \beta J_0 m)}{[\mathrm{e}^{-\Xi} + \cosh(\beta J z \sqrt{q} + \beta J_0 m)]^2}, \quad (11)$$

$$m = \int \mathcal{D}z \, \frac{\sinh(\beta J z \sqrt{q} + \beta J_0 m)}{\mathrm{e}^{-\Xi} + \cosh(\beta J z \sqrt{q} + \beta J_0 m)}. \quad (12)$$

Notice that with a suitable transformation of our parameters ($\beta\mu \to \beta\mu - \ln 2$) we recover the equations obtained using spin-1 variables.

2.1.1. The Case $J_0 = 0$. — The simplest case in this situation corresponds to a zero disordered average, $J_0 = 0$. As can be seen in Figure 1, where the phase diagrams in the plane (T, μ) are depicted for several K, at low temperatures or high values of the chemical potential (high densities), there is a phase transition from a paramagnetic (P; $m = q = 0$) to a spin glass (SG; $m = 0$, $q \neq 0$) phase. For positive values of K (and $J_0 = 0$), these are the only phases allowed to the system. They are separated by a continuous transition up to a tricritical point, T_{trc}, below which a discontinuous transition is observed. We just note that the Sherrington-Kirkpatrick (SK) model with its critical temperature $T_{\mathrm{c}}/J = 1$ is recovered in two limits, both giving the highest possible density ($d = 1$): $\mu \to \infty$ or $K \to \infty$.

We locate the continuous transition by expanding the saddle point equations for small values of q, what leads to

$$\frac{J}{T_{\mathrm{c}}} = 1 + \exp\left(-\frac{K}{J} - \frac{J}{2T_{\mathrm{c}}} - \frac{\mu}{T_{\mathrm{c}}}\right). \quad (13)$$

This equation is valid up to the tricritical point that may be located by expanding the single site partition function around the transition line where $q_{ab} = 0$ and $d_a = \tilde{d}$ [21]. This leads to:

$$\frac{T_{\mathrm{trc}}}{J} = \frac{-3 + 2K/J + \sqrt{9 + 4(K/J)^2 - 4K/J}}{4K/J}. \quad (14)$$

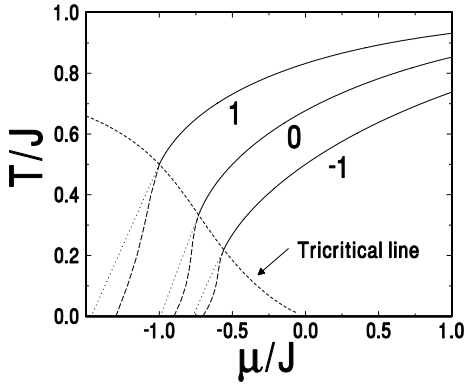

Fig. 1.

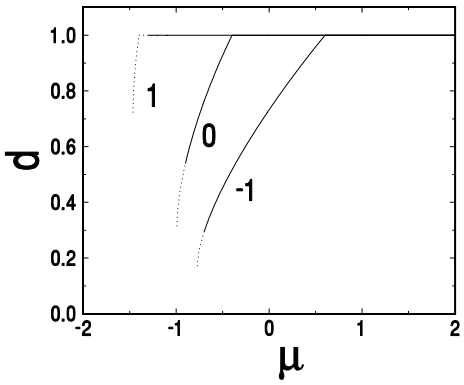

Fig. 2.

Fig. 1. — Phase diagram for several values of K/J showing the paramagnetic (above) and spin glass phase (below the line). The continuous line stands for the second order transition while the long dash line is the discontinuous transition. Also depicted (dotted line) the line where the solution $q \neq 0$ first appears; while the small dash line is a line of tricritical points.

Fig. 2. — The order parameter d at $T = 0$ for $K/J = -1, 0$ and 1. The dotted part signals the region where non zero solution of saddle point equations first appears. Observe that there is a particular value of the chemical potential, μ^*, where the density becomes lower than 1.

For instance, if $K/J = -1$ we get $T_{\rm trc}/J = (5 - \sqrt{17})/4 \simeq 0.219$ and $\mu_{\rm trc}/J \simeq -0.559$ [14]. The line $T_{\rm trc}(K)$ is also shown in Figure 1.

The exploration of our equations in the $T = 0$ limit offers a simple tool to understand the subtle properties of the phase diagrams reported above. Moreover, remembering that our model shares features with the frustrated percolation where no frustrated loops may be closed, it is interesting to study the behavior of the density d at $T = 0$. This behavior is depicted in Figure 2. At $T = 0$ the saddle point equations become:

$$d = \mathrm{erfc}\left[-\frac{1}{\sqrt{2d}}\left(\frac{1}{2}C + \frac{K}{J}d + \frac{\mu}{J}\right)\right], \tag{15}$$

where $C \equiv \beta J(d - q)$ and:

$$C = \sqrt{\frac{2}{d\pi}}\exp\left[-\frac{1}{2d}\left(\frac{1}{2}C + \frac{K}{J}d + \frac{\mu}{J}\right)^2\right]. \tag{16}$$

Actually, d satisfies these equations up to μ^* given by

$$\mu^* = -K - \frac{J}{\sqrt{2\pi}}, \tag{17}$$

below which the close packing configuration is never achieved ($d < 1$); above μ^*, $d = 1$ and $C = \sqrt{2/\pi}$. The point μ^* (see Fig. 2) individuates a clear cusp in the behavior of $d(\mu)|_{T=0}$ and seems to be a characteristic value for the system. We also observe that for high values of K, $K > \sqrt{2/\pi}$, the region with $0 < d < 1$ disappears.

From the tricritical point other two lines depart in the plane (μ, T) (see Fig. 1). They correspond to a thermodynamic line of discontinuous transitions from a paramagnetic to a SG

phase, located where the free energy of the paramagnetic and spin glass solution are equal; and a purely dynamical transition line whose presence is due to the large number of TAP metastable states [22] which can trap the system for very long times (infinite time in the mean field model) [24,25]. The study of this metastable glassy states within a suitable generalization of the TAP approach to the present model is in progress [23].

In order to identify the dynamical transition line we should compute the smallest eigenvalue (replicon) of the 1RSB stability matrix and impose the marginality condition [26]. An alternative procedure amounts to expand the 1RSB free energy (see appendix) around the point $m = 1$, where m denotes here the size of diagonal blocks in the Parisi ansatz [19]. However at level of the approximation we work (replica symmetry) we can guess that the dynamical transition line is located near the line where a non zero solution of replica symmetric saddle point equations first appears; however, to check this point a more detailed investigation will be need.

When the temperature and chemical potential are close enough to the discontinuous transition line we expect that the glassy phase of the system is exactly described by only one step of replica symmetry breaking [23]. On the other hand, when $\mu \to \infty$ (the SK model), the full RSB scheme, with infinite steps, is needed in order to obtain the correct answer. Thus, a further "replica transition line" from a SG phase with one (or finite) replica symmetry breaking level to a SG phase with infinite levels of replica breaking is expected to start at the tricritical point and terminate on the $T = 0$ axis in some characteristic point, probably near μ^*. This transition line is expected to separate qualitatively different *aging* behaviors of the system [27–29].

We can also apply a magnetic field to the system by including a term like $-h \sum_i S_i n_i$ to the Hamiltonian (1) (this is done by adding the term βm to the argument of the hyperbolic functions in the saddle point equations). The continuous transition is destroyed as soon as $h \neq 0$ and the first order transition ends in a critical point, the system presenting the characteristic wing shaped phase diagram. The effects of a magnetic field, as well as the stability of the RS solution in its presence were extensively studied for the Ghatak-Sherrington model [13].

2.1.2. The Case $J_0 \neq 0$. — Having given some details for the case $J_0 = 0$, we face below the more general situation when J_0 is different from zero [32]. There are now three kind of phases (see Fig. 3): a paramagnetic and a spin glass phase with essentially the same characteristics we have discussed above, along with a ferromagnetic phase (F; $q \neq 0$, $m \neq 0$) which appears, as usual, in the low temperature region (or high μ) when $J_0 \gg J$. As in the SK model, this ferromagnetic phase is reentrant (in RS), although here the degree of reentrance may vary.

When the transitions between these phases are continuous (*e.g.*, Fig. 3), the boundary lines may be analytically obtained. The boundary between F and P is given by

$$\frac{J_0}{T_c} = 1 + \exp\left(-\frac{\mu}{T_c} - \frac{K}{J_0} - \frac{1}{2J_0T_c}\right), \tag{18}$$

while the boundary between SG and F obeys

$$T_c = J_0(d - q), \tag{19}$$

where d and q are obtained solving the saddle point equations with $m = 0$. And the boundary between SG and P is our former result (Eq. (13)). Notice that in the limit μ (or K) $\to \infty$, we recover the SK boundaries ($T_c = J$ for SG-P, $T_c = J_0$ for F-P and $T_c = J_0(1 - q)$ for SG-F).

Changing the value of the chemical potential the transitions may become discontinuous, as can be seen in Figure 4 for $\mu = -0.6$ and $K = -1$, where a tricritical point and an endpoint show up.

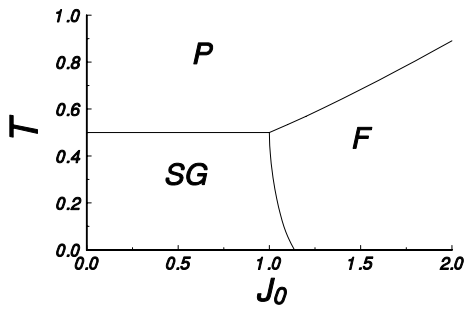

Fig. 3.

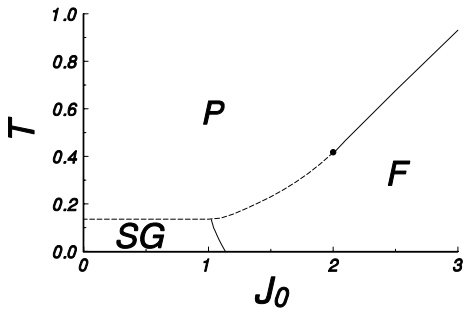

Fig. 4.

Fig. 3. — Phase diagram for $K = -1$ and $\mu = 0$. The reentrance is an artifact of the RS approximation. All transition lines are continuous and look much the same as the SK boundaries.

Fig. 4. — Phase diagram for $K = -1$ and $\mu = -0.6$. The continuous lines are continuous transitions while the dashed lines stand for discontinuous transitions. Notice that the line SG-F ends in an *endpoint* and the transition F-P is discontinuous up to the tricritical point.

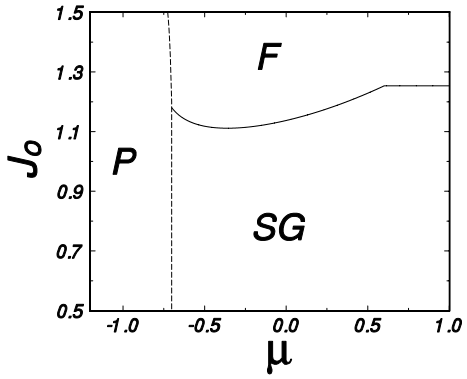

Fig. 5. — Phase diagram at $T = 0$ for $K = -1$ showing the critical *endpoint* when both curves meet.

As usual the analysis at $T = 0$ is interesting. In this limit we get the following equations:

$$d = \frac{1}{2}\mathrm{erfc}\left(\frac{-\frac{1}{2}C - Kd - \mu - J_0 m}{\sqrt{2d}}\right) + \frac{1}{2}\mathrm{erfc}\left(\frac{-\frac{1}{2}C - Kd - \mu + J_0 m}{\sqrt{2d}}\right), \tag{20}$$

$$m = \frac{1}{2}\mathrm{erfc}\left(\frac{-\frac{1}{2}C - Kd - \mu - J_0 m}{\sqrt{2d}}\right) - \frac{1}{2}\mathrm{erfc}\left(\frac{-\frac{1}{2}C - Kd - \mu + J_0 m}{\sqrt{2d}}\right), \tag{21}$$

and

$$C = \sqrt{\frac{2}{d\pi}}\exp\left[-\frac{\left(\frac{1}{2}C + Kd + \mu\right)^2 + J_0^2 m^2}{2d}\right]\cosh\left[-\frac{J_0 m}{d}\left(\frac{C}{2} + Kd + \frac{\mu}{J}\right)\right]. \tag{22}$$

We can then individuate the location of the continuous transition line, in the plane (J_0, μ), between the F and SG phases (Fig. 5). It occurs where $m \to 0$ so, expanding the above

equation in m, we get:

$$J_0 = \sqrt{\frac{\pi d}{2}} \exp\left[\frac{\left(\frac{1}{2}C + Kd + \mu\right)^2}{2d}\right]. \tag{23}$$

Here d and C are evaluated in the points where $m = 0$. This equation is valid up to a given $\mu^* = -K - 1/\sqrt{2\pi}$ (note that since $m = 0$ on this transition line, we just recover our former result) and above this value, we find $J_0 = \sqrt{\pi/2} \simeq 1.253$.

As is well known in the SK model, when J_0 grows too much, the SG phase disappears. A similar phenomenon happens here, but the order of the transition between the phases F and P depends on the value of μ, as expected. Notice that we are considering $K = -1$, but in the next section we will show that for this value there are no antiquadrupolar (glassy or not) phases and the characteristics presented here are also general for greater values of K. We expect that for negative values of K or J_0, there is also the possibility of having ferrimagnetic or anti-ferromagnetic ordering, respectively. The former is characterized by having different magnetizations in the sublattices ($m_{\rm A} \neq m_{\rm B}$) and the latter by having opposite magnetizations ($m_{\rm A} = -m_{\rm B}$). The analysis of these phases is beyond the scope of this paper.

2.2. Repulsive Biquadratic Interaction. — Because the sign of the biquadratic coupling is now negative we have to take into account the possibility of further phase ordering within a two sub-lattice structure. This for instance is the case studied in references [2–6] in absence of quenched disorder and in reference [33] but only for $\mu = 0$. When $\mu \to \infty$ we recover the anti-ferromagnetic Sherrington-Kirkpatrick model, studied in reference [34], and following their prescription, the Hamiltonian can be rewritten as:

$$\mathcal{H} = -\sum_{i,j} J_{ij} S_i^{\rm A} S_j^{\rm B} n_i^{\rm A} n_j^{\rm B} - \frac{K}{N} \sum_{i,j} n_i^{\rm A} n_j^{\rm B} - \mu \sum_{\alpha={\rm A,B}} \sum_i n_i^\alpha, \tag{24}$$

where $\alpha = {\rm A, B}$ is the index of the two sub-lattices. Using the replica method we obtain the following free energy:

$$\begin{aligned} \beta f = \lim_{n\to 0} \frac{1}{n} \Bigg[& \frac{1}{2}\beta^2 J^2 \sum_{a<b} q_{\rm A}^{ab} q_{\rm B}^{ab} + \frac{1}{2}\beta J_0 \sum_a m_{\rm A}^a m_{\rm B}^a \\ & + \frac{1}{4}(\beta^2 J^2 + 2\beta K) \sum_a d_{\rm A}^a d_{\rm B}^a - \frac{1}{2} \ln Z_{\rm A} Z_{\rm B} \Bigg], \end{aligned} \tag{25}$$

where Z_α ($\alpha = {\rm A, B}$) is the single site partition function of the sub-lattice α:

$$\begin{aligned} Z_\alpha = \operatorname*{Tr}_{S,n} \exp \Bigg\{ & \beta^2 J^2 \sum_{a<b} q^{ab} S^a n^a S^b n^b + \beta \sum_a J_0 m^a S^a n^a \\ & + \sum_a \left[\left(\frac{\beta^2 J^2}{2} + \beta K \right) d^a + \beta\mu \right] n^a \Bigg\}. \end{aligned} \tag{26}$$

In the replica symmetric approximation the free energy can be easily computed:

$$\begin{aligned} \beta f = & \frac{1}{2}\beta J_0 m_{\rm A} m_{\rm B} - \frac{1}{4}\beta^2 J^2 q_{\rm A} q_{\rm B} + \frac{1}{4}(\beta^2 J^2 + 2\beta K) d_{\rm A} d_{\rm B} \\ & - \frac{1}{2} \sum_{\alpha={\rm A,B}} \int \mathcal{D}z \, \ln 2 \left[1 + {\rm e}^{\Xi_\alpha} \cosh(\beta J z \sqrt{q_\alpha} + \beta J_0 m_\alpha) \right], \end{aligned}$$

where

$$\Xi_\alpha \equiv \frac{\beta^2 J^2}{2}(d_\alpha - q_\alpha) + \beta K d_\alpha + \beta\mu. \tag{27}$$

From the free energy, one derives the replica symmetric saddle point equations:

$$d_{\rm A} = \int \mathcal{D}z \, \frac{\cosh(\beta J z\sqrt{q_{\rm B}} + \beta J_0 m_{\rm B})}{{\rm e}^{-\Xi_{\rm B}} + \cosh(\beta J z\sqrt{q_{\rm B}} + \beta J_0 m_{\rm B})}, \tag{28}$$

$$q_{\rm A} = \int \mathcal{D}z \, \frac{\sinh^2(\beta J z\sqrt{q_{\rm B}} + \beta J_0 m_{\rm B})}{[{\rm e}^{-\Xi_{\rm B}} + \cosh(\beta J z\sqrt{q_{\rm B}} + \beta J_0 m_{\rm B})]^2}, \tag{29}$$

$$m_{\rm A} = \int \mathcal{D}z \, \frac{\sinh(\beta J z\sqrt{q_{\rm B}} + \beta J_0 m_{\rm B})}{{\rm e}^{-\Xi_{\rm B}} + \cosh(\beta J z\sqrt{q_{\rm B}} + \beta J_0 m_{\rm B})}. \tag{30}$$

The analogous equations for $d_{\rm B}$, $q_{\rm B}$ and $m_{\rm B}$ are obtained from the previous one exchanging A $\leftrightarrow$ B. A representative case is shown in Figure 6 where both $q_{\rm A(B)}$ and $d_{\rm A(B)}$ are presented in the SG and AG phases (see definitions below).

As stated above, new different phases emerge here. At high temperatures (or low μ), when the orientational degrees of freedom are not interacting ($q_{\rm A} = q_{\rm B} = 0$), there are two possible orderings: a paramagnetic (or quadrupolar) phase, P, with $d_{\rm A} = d_{\rm B} \neq 0$ and an antiquadrupolar one, AQ, with $d_{\rm A} \neq d_{\rm B}$. The name quadrupolar is reminiscent from the spin-1 representation ($\tau_i = S_i n_i$) where it labels the ordering of variables $\tau_i^2 = n_i$. At low temperatures (or high μ), the orientational degrees of freedom become important and different glassy phases show up. First, there is a spin glass phase (SG) with $d_{\rm A} = d_{\rm B}$ and $q_{\rm A} = q_{\rm B} \neq 0$. This is the only glassy phase if the effects of particle repulsion are not very strong (K not too negative). On the other side, when K is highly negative, besides the SG phase, there is also an antiquadrupolar glass phase, AG, where the sub-lattice symmetry is broken ($d_{\rm A} \neq d_{\rm B}$, $q_{\rm A} \neq q_{\rm B}$).

As in the previous section, when J_0 is allowed to be nonzero, the system develops a magnetization and additional, ordered phases may appear: when $J_0 \gg J$ at low temperatures (or high μ) a ferromagnetic phase (F; $m_{\rm A} = m_{\rm B} \neq 0$, $d_{\rm A} = d_{\rm B}$, $q_{\rm A} = q_{\rm B} \neq 0$) is encountered if K is not too negative, or either a ferrimagnetic phase is entered (I; $m_{\rm A} \neq m_{\rm B}$, $d_{\rm A} \neq d_{\rm B}$, $q_{\rm A} \neq q_{\rm B}$). Also, with $J_0 \ll -J$, an anti-ferromagnetic phase ($m_{\rm A} = -m_{\rm B} \neq 0$) may shows up.

From now on we consider $J_0 = 0$. As we decrease K from a positive value, there is a point, $K_{\rm AG} \simeq -1.46$, where the AG phase first appears, growing inside the previously described SG phase (see Fig. 7). At a characteristic value, $K_{\rm AQ} = -3/2 - \sqrt{2} \simeq -2.91$, an antiquadrupolar phase appears between the paramagnetic, the SG and the AG phases, as depicted in Figure 8. This value is obtained noticing that there are two points where the P-AQ line intercepts the AQ-SG line (see Fig. 8), given by

$$T_\pm = \frac{1}{2K}\left(K + \frac{1}{2} \pm \sqrt{K^2 + 3K + \frac{1}{4}}\right). \tag{31}$$

When both are equal, we get $K_{\rm AQ}$. As soon as the AQ phase appears, the SG phase is divided in two regions. At even lower values of K (see Fig. 9), the AQ grows, while the left SG phase shrinks and the right one moves to higher values of μ. This SG phase disappears as $K \to -\infty$. We can also notice that the AG phase is invaded by the AQ as we approach this limit, and eventually we have only the P and AQ phases, as we could expect since in this limit we have a lattice gas with repulsive interactions.

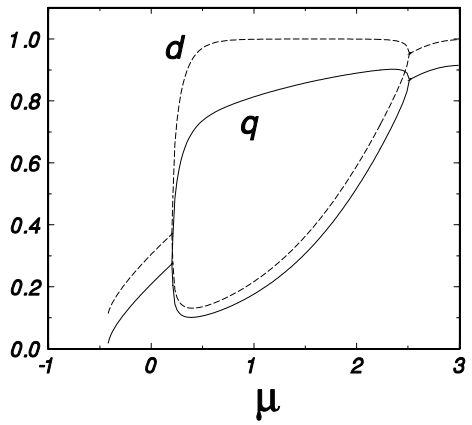

Fig. 6.

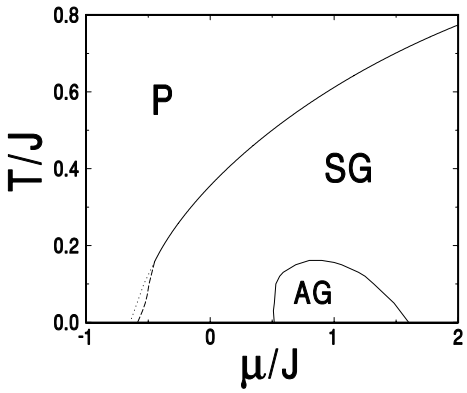

Fig. 7.

Fig. 6. — Plot of the order parameters q (solid line) and d (dashed line) as a function of the chemical potential μ for $K/J = -3$ and a fixed temperature ($T = 0.1$). Both SG and AG phases are presented. In particular, the AG solution is the region were both q and d are twofolded. This figure is an horizontal cross section of Figure 8.

Fig. 7. — Phase diagram for $K = -2$ showing the phase AG. Notice that at this point there is no AQ phase yet.

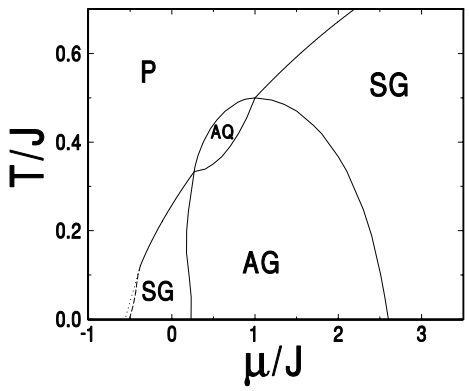

Fig. 8.

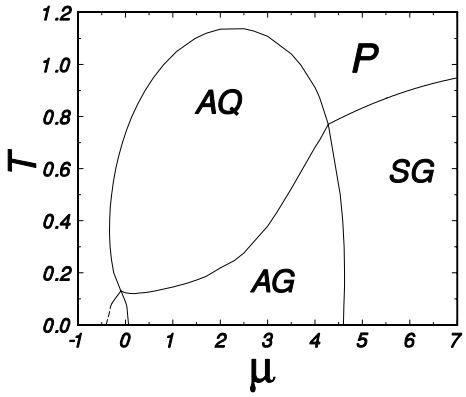

Fig. 9.

Fig. 8. — Phase diagram for $K = -3$ where the AQ phase can be seen. This phase appears when the AG border touches the SG-P transition line for the first time.

Fig. 9. — Phase diagram for $K = -5$ showing the behavior of the various phases for increasing values of K (compares with Figs. 7 and 8).

With the same techniques adopted in the previous paragraph, we can analytically locate the P-AQ continuous transition line reported in Figures 8 and 9:

$$\frac{1}{2}\beta^2 J^2 + \beta K = \frac{1}{d(d-1)}, \tag{32}$$

where d satisfies the equation:

$$d \exp\left(\frac{1}{1-d}\right) = (1-d)\exp(\beta\mu). \tag{33}$$

Analogously, the AQ-AG continuous transition line is given by:

$$\frac{T^2}{J^2} = d_{\mathrm{A}} d_{\mathrm{B}}, \tag{34}$$

where d_{A} and d_{B} satisfy the saddle point equations with $q_{\mathrm{A}}= q_{\mathrm{B}}=0$.

Finally, the AG-SG transition line can be found expanding the saddle point equations in the small quantities q_{A}-q_{B}, d_{A}-d_{B}, representing the staggered order parameter.

The stability of the solutions presented here can be studied by evaluating the eigenvalues of the matrix of Gaussian fluctuations. The eigenvalues structure is analogous to the one found in the SK model [30, 31] with non zero magnetic field since here the chemical potential plays a similar role [14, 32, 33]. However, in this case the eigenvalues may be negative or even complex [9,12,33]. The numerical study of their behavior [33] shows that the paramagnetic and antiquadrupolar phases are inside the stability region while both glass phases (AG and SG) are unstable. The critical line P-AQ, P-SG and AQ-AG are found to be in the stability region, their location depending on the chemical potential, and should not change when replica symmetry is broken; while the transition line AG-SG is found to be completely inside the instability region and its precise location, beyond the aims of this paper, may be found only within the Parisi scheme of RSB.

3. Conclusions

We have studied the global phase diagram of a spin glass version of the Blume-Emery-Griffiths model where the bilinear couplings are quenched Gaussian random variables. The particles, besides the steric effects due to complex molecular structure (represented by the possible spin orientations), are subject to a potential that may be either attractive or repulsive. These steric effects that prevent close packing configuration are common in materials like glasses and poured sand.

This model displays a large variety of interesting critical behaviors. When the particles interaction is attractive or weakly repulsive the transition between the paramagnetic and spin glass phase may be either continuous or discontinuous, depending on the value of the chemical potential; these different behaviors are separated by a tricritical line. For strong repulsive interaction between particles, new different phases with a sub-lattice structure emerge: the antiquadrupolar and the antiquadrupolar glassy phase. These phases seems to be separated by a continuous transition whatever is the value of the chemical potential (at least in the range of K studied here). When the quenched disorder is not symmetrically distributed, also a ferromagnetic phase or a ferrimagnetic phase may appear in the phase diagram.

A further transition line where a dynamical instability appears may also be found as happens in other spin glass models with discontinuous transition. Indeed, many interesting properties emerge if we consider the *dynamical* behavior of systems whose equilibrium properties are described by Hamiltonian (1). For example, the model with diffusive particle dynamics shows strong glassy behavior characterized by diverging relaxation times, vanishing diffusivity and breakdown of the Debye-Stokes-Einstein law [15]; while the spin-1 version of the model with Monte Carlo dynamics displays different aging regimes due to the existence of spin-glass transitions of different nature. In the region where the spin-glass transition is discontinuous

the aging behavior is stable against non-relaxational perturbation [35] and quite similar to the one observed in non-relaxational dynamics of the spherical p-spin glass model [36]. Furthermore when a gravitational term is added to the Hamiltonian (1), strong links appears with granular media and their complex dynamical behavior as logarithmic compaction [37].

Acknowledgments

We are very grateful to R.M.C. de Almeida, A. Coniglio, L. Cugliandolo, J. Kurchan, N. Lemke, Th. Nieuwenhuizen, L. Peliti and S. Salinas for fruitful discussions and comments. We also thank F.A. da Costa for letting us know their results prior to publication and to C.S. Yokoi for providing reference [13]. JJA thanks the warm hospitality of the Dipartimento di Scienze Fisiche at Napoli where this work were started and to CNPq for partial support.

Appendix A

The 1RSB Solution

In this appendix we present the solution of the Blume-Emery-Griffiths spin-glass model with one-step of replica symmetry breaking (1RSB). The following relations are the starting point to get the phase diagram corrections and the dynamical transition line. Without loss of generality we consider the case $J_0 = 0$ where the magnetization is zero. Following the Parisi scheme, the n replicas are divided in n/m blocks containing m replicas. Different replicas in the same block have overlap q_1 while those in different blocks have overlap q_0. Thus, for the case of attractive particles interaction ($K > 0$), the 1RSB free energy reads:

$$\begin{aligned}\beta f_1 &= -\frac{1}{4}\beta^2 J^2\left[(1-m)q_1^2 + mq_0^2 - d^2\right] + \frac{1}{2}\beta K d^2 - \ln 2 \\ &\quad -\frac{1}{m}\int \mathcal{D}z_0\ \ln \int \mathcal{D}z_1\ (1+\mathrm{e}^{\Xi_1}\cosh\Omega_1)^m \end{aligned} \tag{A.1}$$

where:

$$\Omega_1 = \beta J z_0\sqrt{q_0} + z_1\sqrt{q_1 - q_0} \tag{A.2}$$

$$\Xi_1 = \frac{\beta^2 J^2}{2}(d - q_1) + \beta(\mu + Kd). \tag{A.3}$$

The saddle point equations are:

$$d = \int \mathcal{D}z_0 \overline{\left(\frac{\mathrm{e}^{\Xi_1}\cosh\Omega_1}{1+\mathrm{e}^{\Xi_1}\cosh\Omega_1}\right)} \tag{A.4}$$

$$q_0 = \int \mathcal{D}z_0 \overline{\left(\frac{\mathrm{e}^{\Xi_1}\sinh\Omega_1}{1+\mathrm{e}^{\Xi_1}\cosh\Omega_1}\right)^2} \tag{A.5}$$

$$q_1 = \int \mathcal{D}z_0 \overline{\left(\frac{\mathrm{e}^{\Xi_1}\sinh\Omega_1}{1+\mathrm{e}^{\Xi_1}\cosh\Omega_1}\right)^2} \tag{A.6}$$

($d \geq q_1 \geq q_0$) and m satisfies the equation:

$$\begin{aligned}&\frac{1}{4}m^2\beta^2 J^2(q_1^2 - q_0^2) - m\int \mathcal{D}z_0\ \overline{\ln(1+\mathrm{e}^{\Xi_1}\cosh\Omega_1)} \\ &\qquad + \int \mathcal{D}z_0\ \ln\int \mathcal{D}z_1\ (1+\mathrm{e}^{\Xi_1}\cosh\Omega_1)^m = 0.\end{aligned} \tag{A.7}$$

Here the overbar denotes the average:

$$\overline{X} = \frac{\int \mathcal{D}z_1 \, (1 + \mathrm{e}^{\Xi_1} \cosh \Omega_1)^m X}{\int \mathcal{D}z_1 \, (1 + \mathrm{e}^{\Xi_1} \cosh \Omega_1)^m}. \tag{A.8}$$

Following the same procedure, for the case of repulsive particles interaction ($K < 0$) we obtain:

$$\begin{aligned} \beta f_1 = & - \frac{1}{4}\beta^2 J^2 \left[(1-m) q_{1\mathrm{A}} q_{1\mathrm{B}} + m q_{0\mathrm{A}} q_{0\mathrm{B}}\right] \\ & - \frac{1}{4}\left[\beta^2 J^2 + 2\beta K\right] d_{\mathrm{A}} d_{\mathrm{B}} - \ln 2 \\ & - \frac{1}{2m} \sum_{\alpha = A,B} \int \mathcal{D}z_0 \, \ln \int \mathcal{D}z_1 \, A_\alpha^m(z_0, z_1) \end{aligned} \tag{A.9}$$

where:

$$\begin{aligned} A_\alpha(z_0, z_1) &= 1 + \mathrm{e}^{\Xi_{1\alpha}} \cosh(\beta J z_0 \sqrt{q_{0\alpha}} + \beta J z_1 \sqrt{q_{1\alpha} - q_{0\alpha}}) \\ \Xi_{1\alpha} &= \frac{\beta^2 J^2}{2}(d_\alpha - q_{1\alpha}) + \beta(\mu + K d_\alpha). \end{aligned} \tag{A.10}$$

It is straightforward, but tedious exercise, to obtain the saddle point equations.

References

[1] Blume M., Emery V.J. and Griffiths R.B., *Phys. Rev. A* **4** (1971) 1071.
[2] Tanaka M. and Kawabe T., *J. Phys. Soc. Jpn* **54** (1985) 2194.
[3] Osório R., de Oliveira M.J. and Salinas S.R., *J. Phys. C* **1** (1989) 6887.
[4] Hoston W. and Berker A.N., *Phys. Rev. Lett.* **67** (1991) 1027.
[5] Branco N.S., *Physica A* **232** (1996) 477.
[6] Akheyan A.Z. and Ananikian N.S., *J. Phys. C* **29** (1996) 721.
[7] Mézard M., Parisi G. and Virasoro M., Spin Glass Theory and Beyond (World Scientific, Singapore, 1987).
[8] Ghatak S.K. and Sherrington D., *J. Phys. C* **10** (1977) 3149.
[9] Lage E.J.S. and de Almeida J.R.L., *J. Phys. C* **15** (1982) L1187.
[10] Mottishaw P. and Sherrington D., *J. Phys. C* **18** (1985) 5201.
[11] Yokota T., *J. Phys. C* **4** (1992) 2615.
[12] da Costa F.A., Yokoi C.S.O.and Salinas S.R., *J. Phys. A* **27** (1994) 3365.
[13] Yokoi C.S. and Urahata S.M., Proceedings of the Symposium on Statistical Mechanics and Information Sciences, University of Tohoku, Japan (1995) p.53.
[14] Arenzon J.J., Nicodemi M. and Sellitto M., *J. Phys. I France* **6** (1996) 1143.
[15] Nicodemi M. and Coniglio A., *J. Phys. A* (1997) in press.
[16] Coniglio A., *J. Phys. IV France* **3** (1993) C1-1; *Il Nuovo Cimento D* **16** (1994) 1027.
[17] Kirkpatrick T.R. and Thirumalai D., *Phys. Rev. B* **36** (1987) 5388.
[18] Thirumalai D. and Kirkpatrick T.R., *Phys. Rev. B* **37** (1988) 5342 and *Phys. Rev. B* **38** (1988) 4881.
[19] De Santis E., Parisi G. and Ritort F., *J. Phys. A* **28** (1995) 3025.

[20] Crisanti A. and Sommers H.-J., *Z. Phys. B* **87** (1992) 341; Crisanti A., Horner H. and Sommers H.-J, *Z. Phys. B* **92** (1993) 257.
[21] We thank Theo Nieuwenhuizen for pointing this out to us.
[22] Thouless D.J., Anderson P.W. and Palmer R.G., *Philos. Mag.* **35** (1977) 593.
[23] Sellitto M., in preparation.
[24] Bray A.J. and Moore M.A., *J. Phys. C* **13** (1980) L469; Rieger H., *Phys. Rev. B* **46** (1992) 14655.
[25] Kurchan J., Parisi G. and Virasoro M.A., *J. Phys. I France* **3** (1993) 1819; Crisanti A. and Sommers H.-J., *J. Phys. I France* **5** (1995) 805; Kirkpatrick T.R. and Thirumalai D., *J. Phys. I France* **5** (1995) 777.
[26] Sommers H.J., *Z. Phys. B* **50** (1983) 97; Kondor I. and De Dominicis C., *Europhys. Lett.* **2** (1986) 617; Freixa-Pascual M. and Horner H., *Z. Phys. B* **80** (1990) 95.
[27] Cugliandolo L.F. and Kurchan J., *Phys. Rev. Lett.* **71** (1993) 173; *J. Phys. A* **27** (1994) 5749; *Philos. Mag. B* **71** (1995) 501.
[28] Franz S. and Mezard M., *Europhys. Lett.* **26** (1994) 209.
[29] Cugliandolo L.F. and Le Doussal P., *Phys. Rev. E* **53** (1996) 1525.
[30] Sherrington D. and Kirkpatrick S., *Phys. Rev. Lett.* **35** (1975) 1792.
[31] de Almeida J.R.L. and Thouless D.J., *J. Phys. A* **11** (1978) 983.
[32] Schreiber G.R., cond-mat/9612189.
[33] da Costa F.A., Nobre F.D. and Yokoi C.S.O., *J. Phys. A* (1997) in press.
[34] Korenblit I.Y. and Shender E.F., *Sov. Phys. JETP* **62** (1986) 1030; Fyodorov Y.V., Korenblit I.Y. and Shender E.F., *J. Phys. C* **20** (1987) 1835.
[35] Cugliandolo L., Kurchan J., Peliti L. and Sellitto M., In preparation.
[36] Cugliandolo L., Kurchan J., Le Doussal P. and Peliti L., cond-mat/9606060, *Phys. Rev. Lett.*, in press.
[37] Nicodemi M., Coniglio A. and Herrmann H.J., in cond-mat/9606097 and to be published.